EXPERIMENTAL STUDY OF SYNCHROTRON-CERENKOV RADIATION

SLAC Proposal E-126

ADDENDUM: February 1978

1. Synchrotron-Cerenkov Radiation Adapted for Particle Discrimination (π/e) and Energy Determination (0.3 GeV $\lesssim$ E $\lesssim$ 10 GeV).

2. Improvement of Krypton Experiment (D) with Channel Cut Silicon Crystal Monochromators.

1. Synchrotron-Cerenkov Radiation Adapted for Particle Discrimination and Energy Determination.

One of the simplest methods of exploiting synchrotron-Cerenkov radiation for high energy counters is based on the existence of an energy-dependent low frequency cut-off in the spectrum cf. "Experimental Aspects of Synchrotron-Cerenkov Radiation," Ann. Phys. 102, 405 (1976) - Section 3. The essential features can be concisely illustrated by the following examples: Let us first recall the standard form of the S-C spectrum, i.e. the number of photons emitted per unit path per unit energy interval

$$\frac{d^2N^{SC}}{d(\hbar\omega)dL} = \frac{\alpha\sqrt{3}}{2\pi}\frac{H}{H_{cr}}(\lambda_c\hbar\omega)^{-1}\frac{\kappa\left[\frac{\omega}{\omega_c}\left(1+\left(\frac{\omega_o}{\omega}\right)^2\right)^{3/2}\right]}{\left[1+\left(\frac{\omega_o}{\omega}\right)^2\right]^{1/2}} \tag{1.1}$$

where ω_o is the relativistically boosted plasma frequency

$$\omega_o = \omega_p(E/mc^2) \ , \tag{1.2a}$$

ω_c is the characteristic synchrotron frequency

$$\omega_c = \frac{3}{2}E\frac{E}{mc^2}\frac{H}{H_{cr}} \ , \tag{1.2b}$$

and κ denotes the standard synchrotron function

$$\kappa(x) = x\int_x^\infty dz\, K_{5/3}(z) \ . \tag{1.2c}$$

In first approximation we will suppose that the counters are only sensitive to photons for which $\omega(\text{keV}) \gtrsim 0.054\, Z^2$ where Z is the atomic number of the medium. Then from (1.1) we may determine the total S-C photon radiation

rate by simple quadrature, i.e.

$$\frac{dN^{SC}}{dL} = \frac{\sqrt{3}}{2\pi}\frac{\alpha}{\lambda\!\!\!^{-}_c}\int_0^\infty dx\,\frac{K[x^{-2}(x^2+\xi^2)^{3/2}]}{(x^2+\xi^2)^{1/2}} \tag{1.3}$$

where

$$\xi = \omega_o/\omega_c \ . \tag{1.4}$$

In vacuum $\xi \to 0$, and we recover the usual synchrotron results, viz.

$$\frac{dN^{S}}{dL} = \frac{5}{4\pi\sqrt{3}}\,\Gamma\left(\frac{1}{6}\right)\,\Gamma\left(\frac{5}{6}\right)\frac{\alpha}{\lambda\!\!\!^{-}_c}\frac{H}{H_{cr}}\ ; \tag{1.5a}$$

or in practical units

$$\frac{dN^{S}}{dL}\ (\text{photons/meter}) \simeq 0.6179\ H(\text{kG})\ . \tag{1.5b}$$

The essential distinction between (1.3) and (1.5a) is the energy dependence. This can be brought out clearly by rewriting (1.3) in the form

$$\frac{dN^{SC}}{dL} = \frac{dN^{S}}{dL}\,G(\xi)\ , \tag{1.6a}$$

where the auxiliary function G is given by

$$G(\xi) = [6\Gamma(7/6)\ \Gamma(11/6)]^{-1}\int_0^\infty dx\,\frac{K[x^{-2}(x^2+\xi^2)^{3/2}]}{(x^2+\xi^2)^{1/2}}\ . \tag{1.6b}$$

The numerical variation of G can be read off Fig. 1. Note that this is a log-log plot, so the quenching which occurs in the vicinity of $\xi \sim 0.3$ is quite drastic: this feature can be used for energy discrimination.

MEASUREMENT OF THE ELASTIC ELECTRON-NEUTRON CROSS SECTION AT HIGH q^2

Spokespeople:

S. Rock

Z. M. Szalata

Personnel:

R. G. Arnold	American University
B. T. Chertok	" "
F. Martin	" "
S. Rock	" "
Z. M. Szalata	" "
B. A. Mecking	University of Bonn

ABSTRACT

We propose to scatter electrons from deuterons in the kinematic regions of elastic nucleon scattering in the range of $2.5 < q^2 < 10$ $(GeV/c)^2$ at the Stanford Linear Accelerator Center End Station A. From these data we will extract the elastic neutron cross section. These measurements will extend the range of q^2 by a factor of 2.5 over previous work. We request 275 hours of running time and three weeks of checkout time.

An additional 135 hours is requested to measure the elastic e-D cross section at $q^2 = 5.5$ $(GeV/c)^2$.

INTRODUCTION

The internal electromagnetic structure of the elementary particles has been an exciting field for experimental and theoretical research for many years. Many new phenomena have been predicted on the basis of measured elastic and inelastic form factors of the nucleons, e.g. the ρ meson from vector dominance in 1957 and more recently the parton model from the deep inelastic structure functions. The new vector mesons being discovered in $e^+ e^-$ colliding beams $(\rho', \rho'', \omega', \omega'')$ are being used to fit the elastic nucleon form factors using vector dominance models[1]. Quark models are also predicting neutron and proton elastic form factors[2]. Yet the experimental situation for the elastic form factors of the nucleons is far from complete.

The elastic cross section for e-nucleon scattering can be described by "electric" G_E and "magnetic" G_M form factors which are functions of q^2 only.

$$d\sigma/d\Omega = \sigma_{Mott} \cdot \left((G_E^2 + \tau G_M^2) / (1 + \tau) + 2 \tau G_M^2 \cdot \tan^2 \theta/2 \right),$$

where $\tau = q^2/4M_n^2$ and $q^2 > 0$ in the spacelike region.

While the cross section for elastic e-p scattering has been measured[3] for $q^2 < 33$ $(GeV/c)^2$, G_E and G_M have been separately measured[4] only for $q^2 < 3.5$ $(GeV/c)^2$. The corresponding limits for the neutron[5] are 4.0 $(Gev/c)^2$ and 2.7 $(GeV/c)^2$.

Since the newly discovered vector mesons have masses approaching 2 GeV/c^2, the experimentally explored region does not reach the asymptotic limits of the form factors. Moreover, existing quark model predictions and vector dominance fits diverge sharply beyond the measured experimental domain.

MODELS FOR FORM FACTORS

There are two notations for the elastic form factors of the nucleons. The Dirac and Pauli form factors F_1 and F_2 are the structure functions associated with the Dirac term $F_1 \gamma$ and the Pauli (anomalous moment) term $F_2 \cdot \vec{\sigma} \cdot \vec{p}$ in the current. Hence a Dirac particle with no anomalous moment would have $F_2 = 0$. A particle with no charge structure (everywhere neutral) would have $F_1 = 0$. Alternatively, the electric and magnetic form factors G_E and G_M may be used. In the Breit Frame, $G_E(q^2)$ and $G_M(q^2)$ are the Fourier transforms of the charge and magnetic moment distributions of the particle. In the rest frame of the nucleon there is no such simple interpretation.

The relationships between the F's and G's are defined to be:

1) $G_E = F_1 - \tau \cdot F_2$

2) $G_M = F_1 + F_2$

3) $F_1 = (G_E + \tau \cdot G_M)/(1 + \tau)$

4) $F_2 = (G_M - G_E)/(1 + \tau)$

The charge and magnetic moments of the nucleons determine the form factors at $q^2 = 0$.

5) $F_{1n}(0) = 0$

6) $F_{2n}(0) = \mu_n = -1.91$

7) $G_{En}(0) = 0$

8) $G_{Mn}(0) = \mu_n = -1.91$

9) $F_{1p}(0) = 1$

10) $F_{2p}(0) = \mu_p - 1 = 1.79$

11) $G_{Ep}(0) = 1$

12) $G_{Mp}(0) = \mu_p = 2.79$

From the definitions 1) and 2).

$$13)\quad G_E\,(-4M_n^2) = G_M\,(-4M_n^2)$$

The charge radius (second moment of the charge distribution) of the neutron can be shown[6] to be:

$$14)\quad \frac{1}{6}\langle R_n^2\rangle = -\left.\frac{dG_{En}}{dq^2}\right|_0 = -\left.\frac{dF_{1n}}{dq^2}\right|_0 + \frac{F_{2n}(0)}{4M_n^2}$$

$$= -\left.\frac{dF_{1n}}{dq^2}\right|_0 + \frac{\mu_n}{4M_n^2} = -\left.\frac{dF_{1n}}{dq^2}\right|_0 - .543\ (\mathrm{GeV/c})^{-2}.$$

Experimentally[7] $\left.\dfrac{dG_{En}}{dq^2}\right|_0 = .514 \pm .01\ (\mathrm{GeV/c})^{-2}.$

So $\left.\dfrac{dF_{1n}}{dq^2}\right|_0$ is consistent with zero.

Many scaling and other laws have been predicted theoretically or fitted phenomenologically to the data:

i $G_M = \mu/(1 + q^2/.71)^2$ dipole law (Ref. 8).

ii $G_{Ep} = G_{Mp}/\mu p$ form factor scaling (Ref. 9, 10).

iii $G_{Mn} = \dfrac{\mu_n}{\mu_p} \cdot G_{Mp}$ form factor scaling (Ref. 10).

iv $G_{En} = 0$ (Ref. 9).

v $F_{1n} = 0$ (Ref. 11).

vi $\lim_{q^2 \to \infty} F_1(q^2) = C_1/q^4$

$\lim_{q^2 \to \infty} F_2(q^2) = C_2/q^6$ (Ref. 11).

vii a) $F_{1n}/F_{1p} = -1/2$ (Ref. 11).

b) $F_{1n}/F_{1p} = -1/3$ (Ref. 12).

The "laws" i to vii are inconsistent with each other and with some basic definitions 1 to 14 as follows:

i The dipole law is an approximation ($\pm$ 5%) to the data for G_{Mp} for $q^2 < 3.5$ (GeV/c)^2. Beyond that one must evoke (ii) (known to be wrong) to extract G_{Mp} from the cross sections. At $q^2 = 20$ (GeV/c)^2 the dipole fit for G_{Mp} is about 20% higher than the "data". (See Figure 1a). The dipole form agrees with G_{Mn}. (See Figure 1c.)

ii The relation $G_{Ep} = G_{Mp}/\mu_p$ can be derived from a static SU6 model[8]. However, it is inconsistent with Eq. 13 when continued to the time-like region. It is empirically verified for $q^2 < 1.0$ (GeV/c)^2 within the 5% experimental errors. For $q^2 > 1.5$ (GeV/c)^2 the errors are greater than 20% and a violation by as much as 50% ($G_{Ep} < G_{Mp}/\mu_p$) for $q^2 > 2$ is more probable than the dipole law. (See Figure 1b).

iii The relation $G_{Mn} = \mu_n/\mu_p\ G_{Mp}$ is an approximation based on the assumption that isoscalar and isovector form factors both scale. It is consistent with the data for $q^2 < 2.0$ (GeV/c)^2 to within the 10% experimental errors and for $q^2 = 2.7$ to within the 30% errors.

iv The relation $G_{En} = 0$ can be derived from the same SU6 model[9] as (ii) It also cannot be exact since the slope of G_{En} with respect to q^2 is experimentally non-zero (Eq. 14). Empirically G_{En} is consistent with zero for $1.0 < q^2 < 2.7$ (GeV/c)^2 but is positive (.05) for $.1 < q^2 < 1.$ (GeV/c)^2. (See Figure 1d.)

v. The relation $F_{1n} = 0$ is a consequence of a completely neutral neutron. For example, in a 3 quark neutron with all three quarks having the same wave function, the expectation value of the charge is everywhere zero. The Dirac term is just the coherent sum of the Dirac terms of the three quarks, each of which is proportional to the quark charge. Hence the sum is zero. The Pauli term F_{2n} is weighted by the spins and so is non-zero in this model. Equation 14, with $F_{1n} = 0$ is consistent with the data. Eq. 1 and Eq. 2 imply $G_{En} = -\tau G_{Mn}$. This is almost consistent with the data and with condition (13). (See Figure 1d.)

vi. The asymptotic limits are predicted by Brodsky-Farrar[13] from dimensional scaling. It is consistent with the scaling laws i and ii since it yields a $1/q^4$ dependence for those form factors. If $F_{1n} \neq 0$ then it is also consistent with (iii). It is consistent with (iv) if $C_{1n} = C_{2n}$.

vii. The ratios F_{1n}/F_{1p} come from explicit models of the quark wave functions. In viia (viib) only the same flavor (spin) quarks occupy the high momentum region for the scattering. The quark wave functions also determine the ratio of $\nu W_2^n/\nu W_2^p$ at $x = 1$. Models v, viia and viib predict .67, .25 and .43 respectively for this ratio. The experimental results are sensitive to the deuteron corrections[14] on the neutron data and the ratio ranges between 0.25 and 0.4.

The value of the ratio of the neutron to proton cross sections, assuming small angle scattering is:

$$\sigma_n^d/\sigma_p^d = (G_{En}^2 + \tau\ G_{Mn}^2)/(G_{Ep}^2 + \tau\ G_{Mp}^2)$$

$$= (F_{1n}^2 + \tau\ F_{2n}^2)/(F_{1p}^2 + \tau F_{2p}^2)$$

Combining these "laws" in various ways yields different values of the ratio. The limits are for $q^2 \to \infty$.

a) Assume (ii, iii, iv), then:

$$\frac{\sigma_n^{el}}{\sigma_p^{el}} = \frac{\tau\mu_n^2}{1 + \tau\mu_p} \to \frac{\mu_n^2}{\mu_p^2} = .5$$

b) Assume (ii, iii, v), then:

$$\frac{\sigma_n^{el}}{\sigma_p^{el}} = \frac{\tau(1 + \tau)\ \mu_n^2}{1 + \tau\ \mu_p^2}$$

$$\longrightarrow (1 + \tau)\ \mu_n^2/\mu_p^2 = .5\ (1 + \tau)$$

c) Assume (vi) with $F_{1n} \neq 0$, then:

$$\sigma_n^{el}/\sigma_p^{el} \to (C_{1n}/C_{1p})^2$$

with (viia) $\longrightarrow$ 1/4

or (viib) $\longrightarrow$ 1/9

d) Assume (v, vi), then:

$$\frac{\sigma_n^{el}}{\sigma_p^{el}} \to \frac{\tau\ C_{2n}^2/\tau^6}{C_{1p}^2/\tau^4 + \tau\ C_{2p}^2/\tau^6} \longrightarrow \frac{(C_{2n}/C_{2p})^2}{\tau}\ .$$

Thus various reasonable assumptions which are in reasonable agreement with the data yield very different behavior for $\sigma_n^{el}/\sigma_p^{el}$ ranging from linear in τ to $1/\tau$. Figures 2a and 2b show some of these predictions along with some vector dominance models and the existing data at small angles and at $\theta = 45^o$. A high q^2 experiment ($q^2 = 8$ or 10 GeV/c)^2) can clearly distinguish between these various possibilities.

VECTOR DOMINANCE MODELS

There are a wide variety of forms used to express how the vector mesons actually dominate the photon-nucleon interaction. Many share the feature that outside the range of experimental data they become dominated by spurions. Others are more asymptotically bound in that they go over into some of the forms (i) to (vii) at high q^2. The former includes Felst's simple monopole model[1]. If it is modified with an additional form factor for the vector meson-nucleon vertex, we get the dipole forms (i) and (iii). However, since $F_2 \rightarrow 1/q^4$, G_{Ep} and G_{En} will eventually dominate.

Blatnik and Zovko[1] have developed a VDM which includes conditions (vi) and (13). With four free parameters and six vector mesons they then predict $F_{1n}/F_{1p} \rightarrow -.37$ at high q^2 which is between conditions (viia and vii b). Eq. 14 is also approximately satisfied.

The IJL Vector Dominance Model with dipole also satisfies (vi) and Eq. 13, but has $F_{1n}/F_{1p} \rightarrow 4.75$ asymptotically. Figure 2 shows some of these VDM predictions.

QUASIELASTIC SMEARING

The deuteron is a loosely bound proton and neutron, moving around each other with the momentun distribution given by the wave function. In the impulse approximation, scattering is from only one of the nucleons. The other (spectator) nucleon is not affected (except to be nudged onto its mass shell) and flies off with the fermi momentum it had when its companion was struck. Quasielastic scattering is elastic scattering from these quasifree nucleons. Due to the target nucleon being in motion, the missing mass reconstructed from the recoil electron (under the assumption that the nucleon is at rest) will be spread out over several hundred MeV. This same motion of the target nucleons spreads out the inelastic scattering from single nucleons. For example, a small fraction of

the scattering at the first resonance will have a single arm missing mass reconstruction near the nucleon mass. Thus the inelastic scattering region near missing mass $W = M_p$ will have contributions from elastic proton and neutron scattering and from inelastic processes.

A Monte Carlo computer program was built to determine the relative sizes of the inelastic background and elastic signals. Elastic and inelastic cross sections for e-p measured at SLAC[15] were separately smeared using the momentum wave function of the deuteron[16]. The inelastic proton background was multiplied by 1.5 to simulate the inelastic neutron scattering. Some examples of the resulting W distributions are shown in Figures 3 and 4 at q^2 of 5.63 and 8.8 $(GeV/c)^2$. Figure 5 shows the ratio of $\sigma_p^{el}/\sigma_{p+n}^{inel}$ as a function of W for different q^2. While the ratio of elastic to inelastic cross sections declines with increasing q^2, the signal-to-background is still almost 2 to 1 at $W = .94$ GeV/c^2 at $q^2 \approx 9$ $(GeV/c)^2$. These plots do not include the unmeasured neutron elastic cross section (.1 to 1.4 times σ_p^{el}). Figure 6 shows the integrated elastic and inelastic e-p spectra indicating the dominance of the proton quasielastic signal by almost 2 to 1 up to $W = 1.02$ GeV/c^2.

To compare these Monte Carlo smeared inelastic spectra with the real world, preliminary unpublished e-d data from SLAC Group A[15] are shown in Figs. 7 and 8 for $q^2 = 3.7$ and 6.9 $(GeV/c)^2$. Also shown are the smeared e-p elastic and inelastic data. In addition Figure 8 shows the inelastic component. It is clear that a neutron signal is present. A rough evaluation yields $\sigma_n^{el}/\sigma_p^{el} = .4 \pm .1$ and $.5 \pm .2$ for $q^2 = 3.7$ and 6.9 $(GeV/c)^2$ respectively, where the errors are statistical only. The shape of the proton inelastic cross section is similar to that of the deuteron data. They differ by the neutron contribution which is approximately 50% of the proton signal.

There is some theoretical understanding of the inelastic background as well as the shape of the quasielastic peak. Figure 9 shows $q^2 = 1.53$ $(GeV/c)^2$ data[17] compared with the inelastic calculations of Gutbrod and Simon [18] and the quasielastic shape of McGee[19]. These shapes may be used to extract the neutron cross section from the data as they have been on previous neutron form factor experiments, e.g. Ref. 17.

EXPERIMENTAL SETUP

This experiment is typical of single arm measurements made in the End Station A at SLAC and will use mostly existing equipment. No new major components for the experiment will be necessary.

The 20 GeV spectrometer, positioned at 10^o with respect to the beam will be used to detect electrons scattered from deuterium, hydrogen, and empty targets. The spectrometer will be equipped with its usual complement of trigger counters, proportional wire chambers, shower counters and Cerenkov counter for detecting and analyzing the scattered electrons. The spectrometer and beam resolution is more than sufficient to chart out the shape of the quasielastic peak.

The SLAC electron beam will be used in its standard form over the energy range 9 to 21 GeV with momentum defining slits set between .2 and .5%.

The 8 GeV spectrometer, instrumented with p, θ, and ϕ hodoscopes may be used to detect the recoil proton. While the full momentum and angular spread of the proton cannot be covered, this sample of e-p coincidences may be useful in cross checking the Monte Carlo calculations. This is still under study. Two successful experiments using the 20 and 8 GeV spectrometers in coincidence have been done by our group.[20]

The experiment will use an existing target assembly consisting of a set of cylinders remotely controlled. The target cylinders are 30 cm long,

10 cm in diameter with .125 mm end caps. The beam will be offset horizontally from the axis of the cylinder so that all electrons scattered at 10^{o} will exit through the front window.

The signals from the counters and proportional wire chambers will be processed through the standard electronic equipment and the information accumulated by an on-line SDS computer. Some real time analysis will be done on a sample of the data in order to monitor the progress of the experiment. Final data analysis will be done off-line at the SLAC Computer Facility.

EXPERIMENTAL PROGRAM

Quasielastic scattering of electrons off deuterons will be measured at 5 values of q^2. The kinematic parameters are listed in Table I. Since the quasielastic peak is somewhat wider than the momentum acceptance of the spectrometer, three measurements will be made at each q^2 setting with the central momentum value of the spectrometer set 3% above (region III), 3% below (region I) and at the center (region II) of the quasielastic peak (see Figures 10 and 11). This gives a complete picture of the entire peak plus some background above and below for normalization. For purposes of calibration and proton quasielastic subtraction, elastic proton scattering will also be measured at each value of q^2. Using the partially analyzed deuteron data from previous experiments mentioned above[15] and the elastic and inelastic proton cross sections, an estimate has been made of the counting rates at various values of q^2 (Table I).

Apart from systematic error the accuracy achieved depends on the total number of detected events in the quasielastic peak as well as the size of the quasielastic proton contribution and the inelastic backgrounds (b) which must be subtracted. Let P represent the total proton elastic counts from the hydrogen target, while D represents the quasielastic counts from deuterium in a particular bin. Then:

(16) $$\sigma_n = \sigma_d - \sigma_p - \sigma_b$$

(17) $$(\delta\sigma_n)^2 = (\delta\sigma_d)^2 + (\delta\sigma_p)^2 + (\delta\sigma_b)^2$$

(18) $$(\delta\sigma_n/\sigma_n)^2 = \frac{1}{D \cdot f_n^2} + \frac{f_P^2}{P \cdot f_n^2} + \left(\frac{e_b \cdot f_b}{f_n}\right)^2$$

where $f_n = \sigma_n^{el}/\sigma_d$ neutron fraction

$f_p = \sigma_p^{el}/\sigma_d$ proton fraction

$f_b = \sigma_b/\sigma_d$ background fraction

and $e_b = \delta\sigma_b/\sigma_b$ fractional background error.

The background σ_b is estimated from the Monte Carlo smeared inelastic e-p scattering with an additional 50% added on for e-n scattering. (Figures 3, 4 and 8).

Since σ_n is unknown, we have calculated the errors for various values of $\sigma_n^{el}/\sigma_p^{el} = s$, ranging from 0.1 to 0.5. The W range has been divided into bins of 40 MeV with 10 bins covering most of the quasielastic peak. The central bin ($W = .94$ GeV/c^2) contains about 13% of the counts in region II. Figure 12 shows f_n, the neutron fraction, as a function of s and q^2 for the central bin of the quasielastic peak. Many systematic errors cancel or almost cancel by taking the ratio σ_d/σ_p^{el}. These include absolute calibrations of spectrometer acceptance, beam monitors, detector efficiencies, radiative corrections and some rate effects. Other sources of error are final state interactions and uncertainties in the smearing from the deuteron wave function. From the papers of Hanson, Budnitz and Bartel[5], we estimate a 5% systematic error in σ_d/σ_p^{el}. This scales into an error of 5%/s in $\sigma_n^{el}/\sigma_p^{el}$. Table II shows the contributions to the relative error $\delta\sigma_n/\sigma_n$ from counting statistics of 2000 events in the central bin of the quasielastic peak (D) and for $e_b = 10\%$. These errors are added in quadrature with the elastic proton error and systematic errors to give the total error. If possible enough counts will be collected so that the uncertainty in the

background and systematics dominates the error. This will probably be at about the 2000 counts/bin level. The cross section, σ_n can be calculated in each bin (of W) and compared as a check of the background shape.

By overlapping the spectrometer settings for regions I and II (see Figures 10 and 11) and counting for an equal time span in each, the counts obtained per bin becomes a good match to the required counts for uniform sensitivity over a large range of W. Region I covers a region of very low incoherent background and allows an exploration of the tails of the fermi distribution and coherent background processes. Region III requires only half the running time of region II because neutron cross sections cannot be extracted due to the high background and because the total cross sections are much higher. Data in region III will be used to normalize and check the calculated inelastic background.

Table I summarizes the cross sections, rates and required coulombs and hours for the measurement, assuming 2000 counts/bin are collected in the central bins of region II. Included is time for proton calibration measurements to be used to subtract the proton portion of the quasielastic peak and for the inevitable target empty background. Equation 18 was used to calculate the coulombs needed for the proton measurement with the assumption of D = 2000 and the proton error term being about 40% of that from deuterium. In region I there is no proton signal and in region III equal time will be devoted to deuteron and hydrogen measurements to unravel the background.

We request time for measurements at q^2 = 2.5, 4, 6, 8, 10 $(GeV/c)^2$ for a total time of 180 hours. We assume an efficiency factor of 65% for time lost due to target and spectrometer field setting changes, energy changes and equipment failures. This yields a total request of 275 hours.

During data taking, targets and spectrometer settings will be changed

at frequent intervals to assure small relative normalization errors. Polarization experiments[21] have achieved relative normalization errors of better than 1 in 10000 which is far better than we need (2% for 2000 counts).

Figure 13a and 13b show the approximate errors obtainable with a 5% (10%) background error and statistics of about 2000 counts in the central bin and 5% systematic errors (see Table II). Depending on the way the form factors approach their asymptotic values, we may be able to distinguish between models viia and viib. Clearly models which lead to much larger values of $\sigma_n^{el}/\sigma_p^{el}$ can be easily tested by this measurement. Our results will put severe restrictions on any vector dominance or quark model of the nucleon structure as well as providing one of the building blocks for the construction of the form factors of the other nuclei.

APPENDIX A

MEASUREMENT OF HIGH q^2 ELASTIC ELECTRON DEUTERIUM SCATTERING

The deuteron elastic structure functions at large q^2 are an ideal place to study nucleon-nucleon interactions at short distances. $A(q^2)$ has been measured (E-101)[22] up to 6 $(GeV/c)^2$ with events registered up to $q^2 = 4$ $(GeV/c)^2$ and an upper limit set at $q^2 = 6$ $(GeV/c)^2$. These data have prompted many new theoretical investigations. These approaches calculate $A(q^2)$ to be either rapidly falling exponentials[23] $A \propto q \cdot \exp(-8.2q)$ or power laws[24,25] or complicated results from detailed nuclear physics models[26]. Predictions from some of these calculations are compared for $q^2 > 3$ $(GeV/c)^2$ in Figure 14. They differ by almost 2 orders of magnitude at $q^2 = 5.5$ $(GeV/c)^2$. For example, the asymptotic behavior of the deuteron form factor $F = \sqrt{A}$ can be calculated in a 6-component Dimensional Scaling Quark Model (DSQM) using constituent interchange:[23]

$$F_{DSQM} = \frac{C\, F_N^2(q^2/4)}{(1+q^2/1.2\beta^2)} \rightarrow \left(\frac{1}{q^2}\right)^5 \tag{A1}$$

where $F_N(q^2)$ is the nucleon form factor. The ratio of experiment to F_{DSQM} is presented in Figure 15 where one observes a q^2 independence beyond $q^2 = .7$ $(GeV/c)^2$. In the detailed nuclear physics calculations the unknown neutron form factors generate large uncertainties in the calculations of $A(q^2)$ at large q^2. For example, see the different predictions of Gari and Hyuga (GH) on Figure 14. The high q^2 neutron cross sections to be obtained in the main experiment will be used as input for more exact calculations of the deuteron form factors[24].

We propose to make one measurement at about $q^2 = 5.5$ to distinguish between these predictions. We note that the DSQM prediction is 2.5 standard deviations above the datum point at $q^2 = 4$ $(GeV/c)^2$ and differs from the Schmidt-Blankenbecler (SB) prediction by a factor of 3 at $q^2 = 5.5$ $(GeV/c)^2$.

The event sample calculated from the DSQM for 100 hours of beam time at $\theta_e = 8^o$ with full beam intensity and 180 pps would be:

q^2	E_o	Events
5.0	16.71	11
5.5	17.56	5
6.0	18.37	2.5

A running efficiency of 75% would mean 135 hours of SLAC time.

The experimental details of this measurement are well understood from E-101 with an excellent signal-to-noise ratio which permits unambiguous identification of elastic events satisfying both the kinematic and time of flight constraints[22]. With the 20 and 8 GeV spectrometers already set up for the main experiment, there will be little if any additional setup time or support effort needed.

In addition to the elastic data, single arm data measuring

$$\nu W_2^d \quad \text{for} \quad 0.6 < x_d < 1$$

will be logged and this is quite valuable in its own right[27].

We believe that the investment of 135 hours on one data point could have important bearing on the understanding of the deuteron at short distances.

REFERENCES

1. F. Iachello et al., Phys. Lett. 43B (1973) 191
   S. Blatnik and N. Zovko, Acta Physica Austriaca 39 (1974) 62
   F. Felst Desy Preprint 73/56 Unpublished

2. S. Brodsky and B. Chertok, Phys. Rev. D14 (1976) 3003
   P. Fishbane et al., Phys. Rev. D11 (1975) 1338
   R. D. Carlitz, S. D. Ellis and R. Savit, Phys. Lett. 68B (1977) 443
   L. M. Sehgal, Phys. Lett. 53B (1974) 106
   B. Hamprecht, Il Nuovo Cimento 38A (1977) 279
   R. S. Kaushal and D. Parashar, Il Nuovo Cimento 39A (1977) 272

3. D. H. Coward et al., Phys. Rev. Lett. 20 (1968) 292
   W. B. Atwood, SLAC Report 185 (1975)

4. J. Litt et al., Phys. Lett. 31B (1970) 40
   W. Bartel et al., Nucl. Phys. B58 (1973) 429

5. C. W. Akerlof et al., Phys. Rev. 135 (1964) B810
   E. B. Hughes et al., Phys. Rev. 139 (1965) B458
   J. R. Dunning et al., Phys. Rev. 141 (1966) 1286
   W. Albrecht et al., Phys. Lett. 26B (1968) 642
   R. J. Budnitz et al., Phys. Rev. 173 (1968) 1357
   S. Galster et al., Nucl. Phys. B32 (1971) 221
   W. Bartel et al., Nucl. Phys. B58 (1973) 429
   K. Hanson et al., Phys. Rev. D8 (1973) 753

6. F. J. Ernst, R. G. Sachs and K. C. Wali, Phys. Rev. 126 (1962) 2256

7. V. E. Krohn and G. R. Ringo, Phys. Rev. D8 (1973) 1305
E. Melkonian et al., Phys. Rev. 114 (1959) 1571
D. J. Hughes et al., Phys. Rev. 90 (1953) 497
P. M. Fishbane et al., Phys. Rev. D11 (1975) 1338

8. J. Litt et al., Phys. Rev. Lett. 20 (1968) 429

9. K. J. Barnes, P. Carruthers and F. von Hippel, Phys. Rev. Lett. 14 (1965) 82

10. T. Narita, Progress in Theoretical Physics 42 (1969) 1336
A. L. Licht and A. Pagnamenta, Phys. Rev. D4 (1971) 2810

11. S. Brodsky and B. Chertok, Phys. Rev. D14 (1976) 3003

12. G. Farrar and D. Jackson, Phys. Rev. Lett. 35 (1975) 1416

13. S. Brodsky and G. Farrar, Phys. Rev. D11 (1975) 1309

14. W. B. Atwood and G. B. West, Phys. Rev. D7 (1973) 773
Arie Bodek, Phys. Rev. D8 (1973) 2331
Ivan Schmidt and R. Blankenbecler, Phys. Rev. D16 (1977) 1318

15. Private Communications. Les Cotrell and Mac Meysteyer, SLAC

16. H. G. Hilpert et al., Nucl. Phys. B8 (1968) 537

17. W. Bartel et al., Nucl. Phys. B58 (1973) 429

18. F. Gutbrod and D. Simon, Nuovo Cimento 51A (1967) 602

19. I. J. McGee, Phys. Rev. 158 (1967) 1500
I. J. McGee, Phys. Rev. 161 (1967) 1640

20. R. Arnold et al., Phys. Rev. Lett 35 (1975) 776
R. Arnold et al., to be published

21. S. Rock, UCRL Report 20041 (1970)

22. R. Arnold et al., Phys. Rev. Lett. 35 (1975) 776

23. G. B. West, Phys. Rev. Lett. 37 (1976) 1454

24. S. Brodsky and B. Chertok, Phys. Rev. D14 (1976) 3003

25. Ivan Schmidt and R. Blankenbecler, Phys. Rev. D16 (1977) 1318

26. M. Gari and H. Hyuga, Phys. Rev. Lett. 36 (1976) 345,
Nucl. Phys. A264 (1976) 409
R. Arnold, C. Carlson and F. Gross, Phys. Rev. Lett. 38 (1977) 1516

27. W. Schutz et al., Phys. Rev. Lett. 38 (1977) 259
Ivan Schmidt and R. Blankenbecler, Phys. Rev. D16 (1977) 1318

TABLE I

KINEMATICS, CROSS SECTIONS, COUNTING RATES

q^2 $\left(\frac{GeV}{c}\right)^2$	E_o (GeV)	$\left(\frac{d\sigma}{d\Omega}\right)_p^{el}$ (mb)	(a) $\frac{\sigma_p^{el}}{\sigma_b}$	(b) $\left(\frac{d\sigma}{d\Omega}\right)_d$ (mb)	(c) COUNTING RATE (D) (cnts/sec)	(d) TOTAL CHARGE (COUL)	RUNNING TIME (HOURS)
2.5	9.76	8×10^{-6}	> 12	10.0×10^{-6}	40.5	0.01	10
4.0	12.59	1.2×10^{-6}	> 12	1.5×10^{-6}	6.1	0.04	15
6.0	15.74	2.0×10^{-7}	5.0	2.9×10^{-7}	1.2	0.2	15
8.0	18.50	5.0×10^{-8}	2.0	9.0×10^{-8}	0.4	0.8	45
10.0	21.00	1.7×10^{-8}	1.05	3.7×10^{-8}	0.15	1.8	100
					Totals	2.85	185

(a) Central Bin ($W = .94\ GeV/c^2$)

(b) Region II, $\sigma_d = \sigma_n + \sigma_p + \sigma_b = \left(1.25 + \frac{\sigma_b}{\sigma_p}\right)\sigma_p$

(c) Region II, at 5 μA, 30 cm target

(d) Deuterium plus hydrogen plus dummy, all regions, for 2000 deuterium counts in Central Bin ($W = .94\ GeV/c^2$) ≈ 15,000 D_2 counts in Region II.

TABLE II

FRACTIONAL ERRORS $e_n = \frac{\delta\sigma_n}{\sigma_n}$

q^2 $\left(\frac{GeV}{c}\right)^2$	$\sigma_n = 0.5\ \sigma_p$			$\sigma_n = 0.25\ \sigma_p$			$\sigma_n = 0.1\ \sigma_p$		
	BKGND	STAT	TOTAL	BKGND	STAT	TOTAL	BKGND	STAT	TOTAL
2.5	0.01	0.04	0.11	0.01	0.03	0.20	0.03	0.10	0.51
4.0	0.01	0.06	0.12	0.02	0.08	0.22	0.05	0.18	0.53
6.0	0.04	0.08	0.13	0.08	0.13	0.25	0.20	0.29	0.61
8.0	0.10	0.10	0.17	0.20	0.18	0.34	0.50	0.42	0.82
10.0	0.19	0.12	0.25	0.38	0.23	0.49	0.95	0.52	1.19

ASSUMPTIONS

10% Error in inelastic background.

5% Systematic Error scaled by s, see text.

2,000 Counts in central bin of the quasielastic peak.

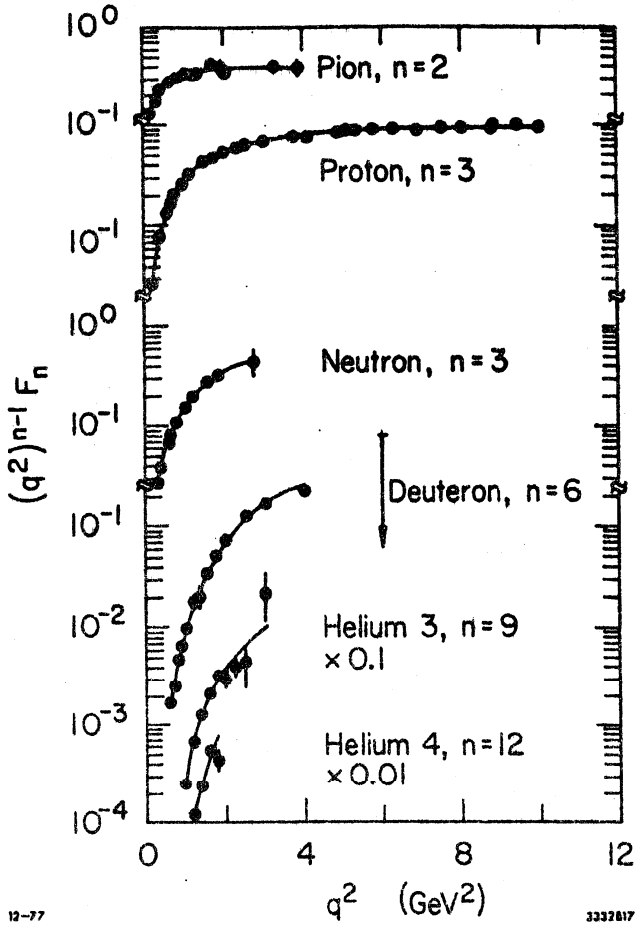

Fig. I1 Elastic hadronic and nuclear form factors displayed by Dimensional Scaling Quark Model with n = number of constituent quarks.

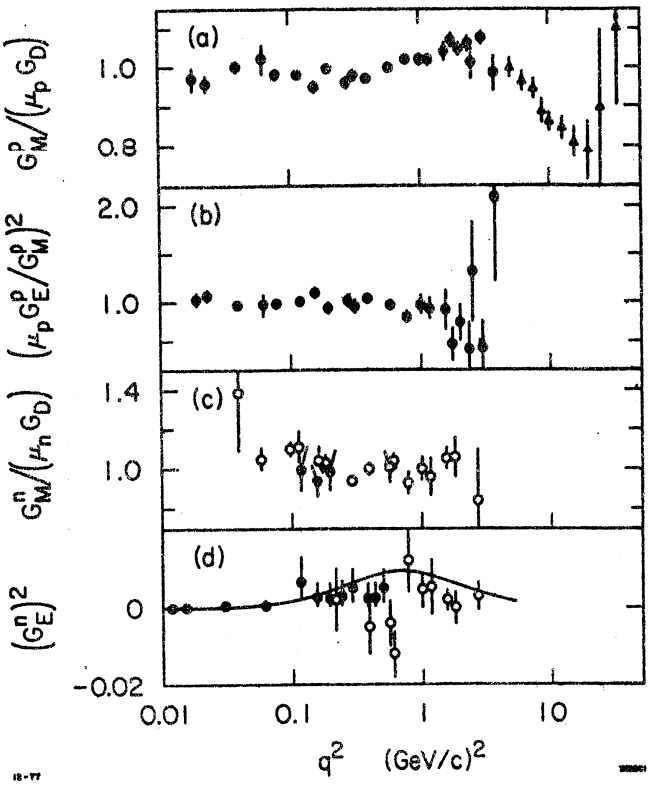

Fig. 1 Existing data for the elastic nuclear form factors. G_D is the dipole form $1/(1 + q^2/.71)^2$.

a) $G_{Mp}/(\mu_p G_D)$

b) $(\mu_p G_{Ep}/G_{Mp})^2$

c) $G_{Mn}/(\mu_n G_D)$

d) $(G_{En})^2$

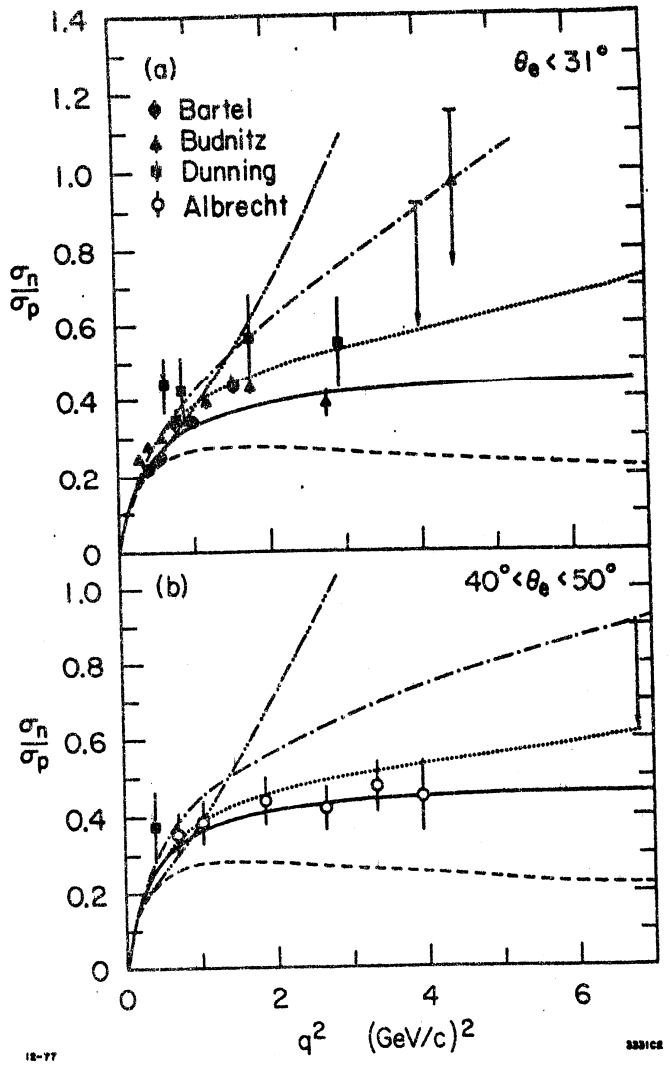

Fig. 2 Existing data and some models for the ratio of elastic neutron and proton cross sections $\sigma_n^{el}/\sigma_p^{el}$.

a) $\theta < 35^o$ i.e. $\tan^2\theta/2 \ll 1$

b) $40^o \leq \theta \leq 50^o$

The curves are:

——— Assumption a in the text.

—·—·— Assumption b in the text.

– – – – VDM model of Blatnik and Zovko (Ref. 1)

—··—··— VDM model of IJL (Iachello et al., Ref. 1)

····· Veneziano type model of Felst (Ref. 1)

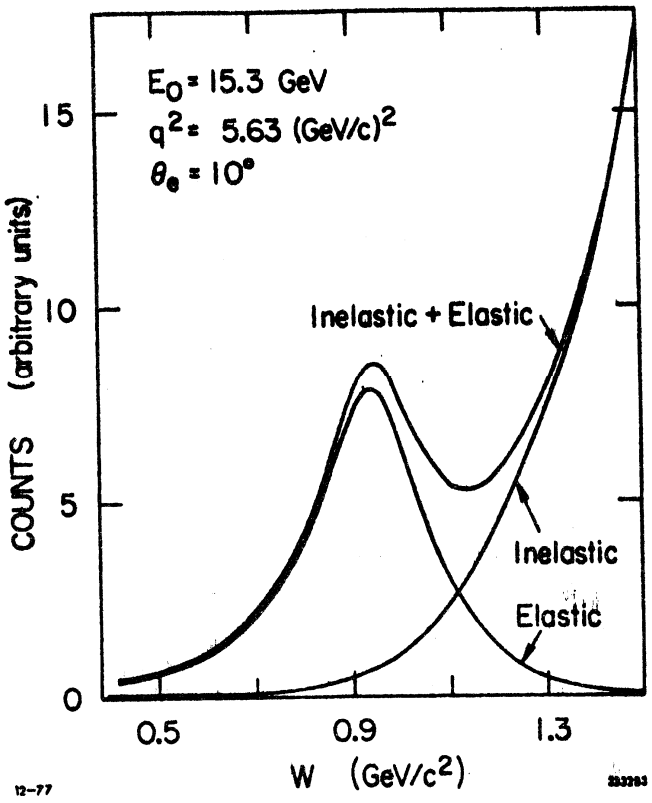

Fig. 3 Quasielastic proton and inelastic proton cross sections smeared by the Monte Carlo, and the sum as a function of invariant mass W at q^2 = 5.63 (GeV/c)^2. The inelastic spectrum is the smeared measured proton inelastic cross section times 1.5 for the neutron component.

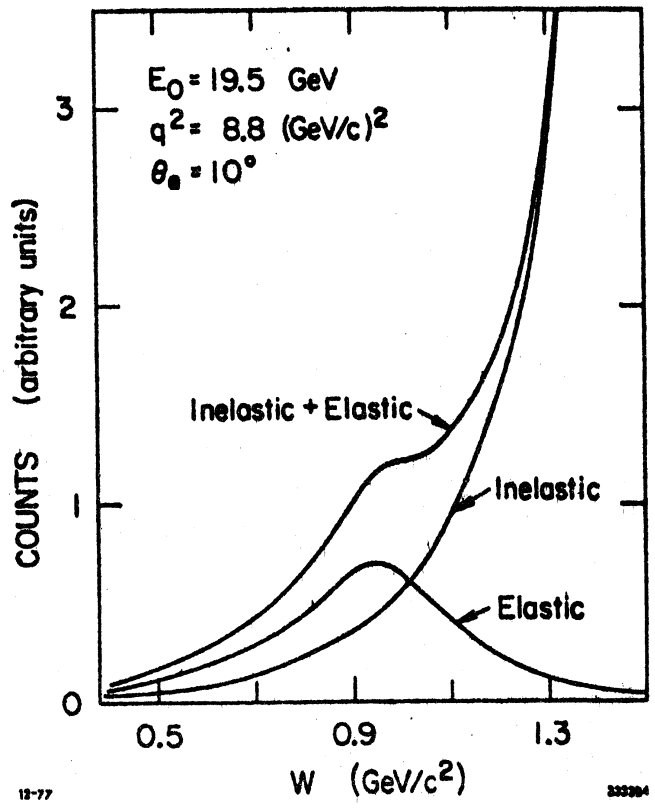

Fig. 4 Quasielastic proton and inelastic proton cross sections smeared by the Monte Carlo, and the sum as a function of invariant mass W at q^2 = 8.8 (GeV/c)^2. The inelastic spectrum is the smeared measured proton inelastic cross section times 1.5 for the neutron component.

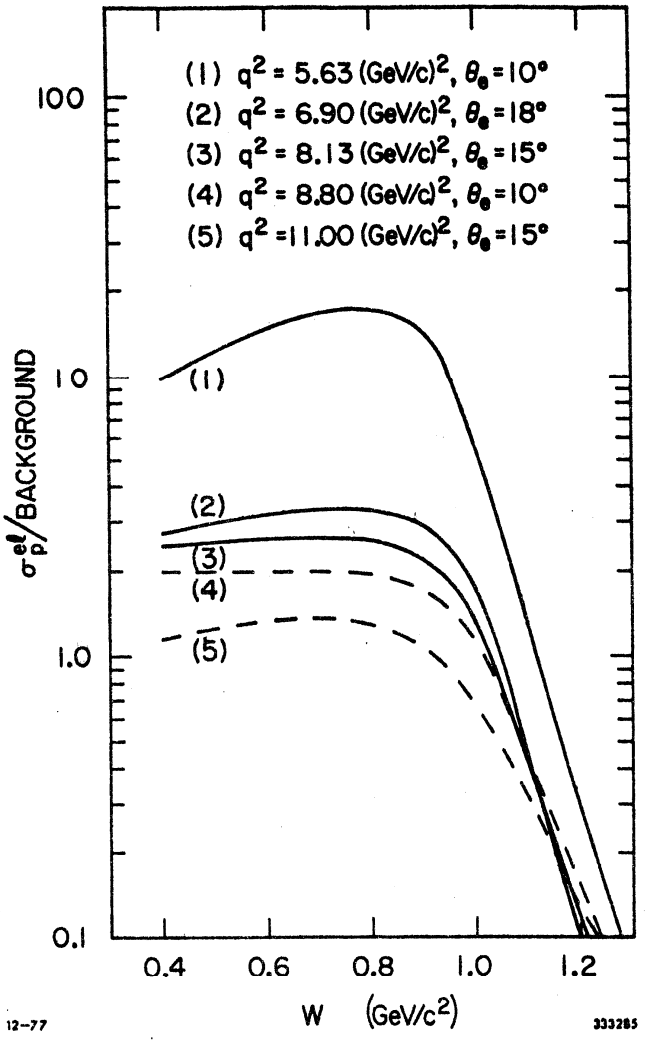

Fig. 5 Ratio of proton quasielastic to inelastic background cross sections as a function of W. The background is 1.5 times the measured smeared proton inelastic data (Ref. 15).

The curves are for 1) q^2 = 5.63 (GeV/c)^2
2) q^2 = 6.9 (GeV/c)^2
3) q^2 = 8.13 (GeV/c)^2
4) q^2 = 8.8 (GeV/c)^2
5) q^2 = 11.0 (GeV/c)^2

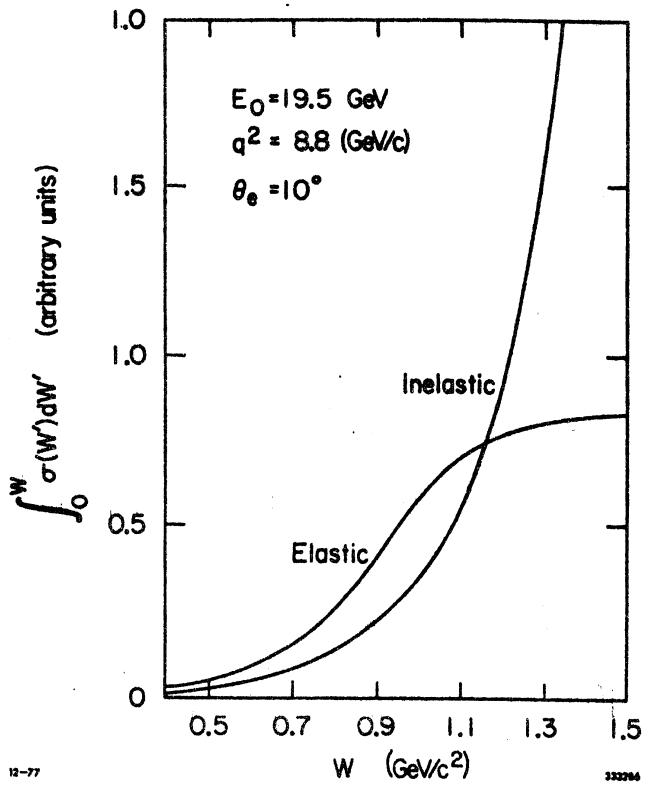

Fig. 6 The integral of the elastic and inelastic cross section curves at $q^2 = 8.8$ GeV/c)^2 in Fig. 4, summed from W = 0 GeV/c^2.

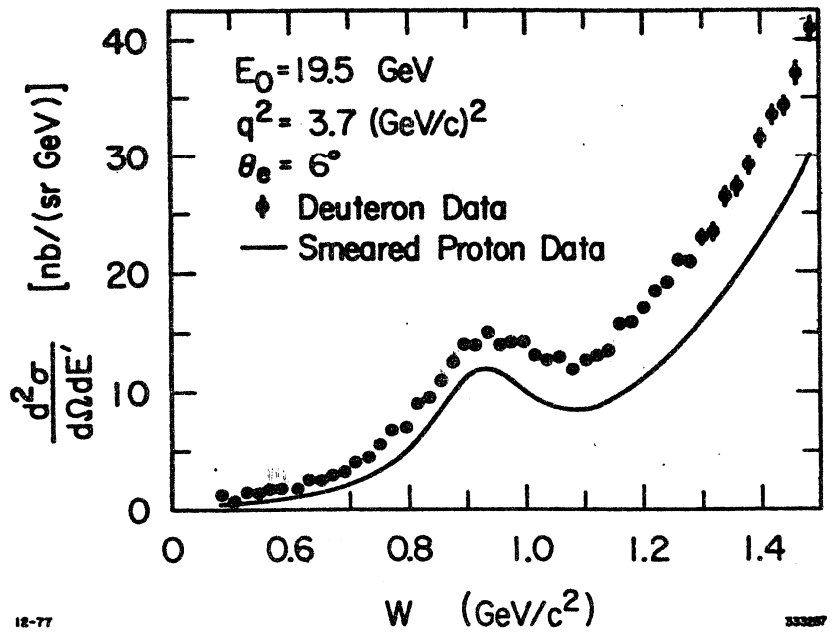

Fig. 7 Deuteron cross section data (points) (Ref. 15) and Monte Carlo smeared e-p elastic plus inelastic data (curve) (Ref. 15) as a function of W for q^2 = 3.7 $(GeV/c)^2$

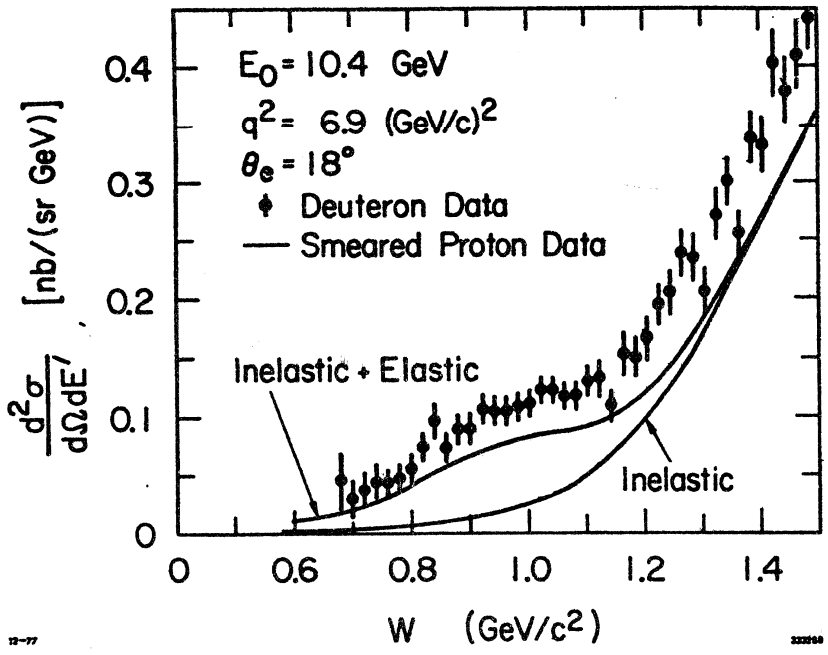

Fig. 8 Deuteron cross section data (points) (Ref. 15), Monte Carlo smeared e-p elastic plus inelastic data (Ref. 15) and the smeared e-p inelastic data(elastic peak and radiative tail removed) all at q^2 = 6.9 $(GeV/c)^2$.

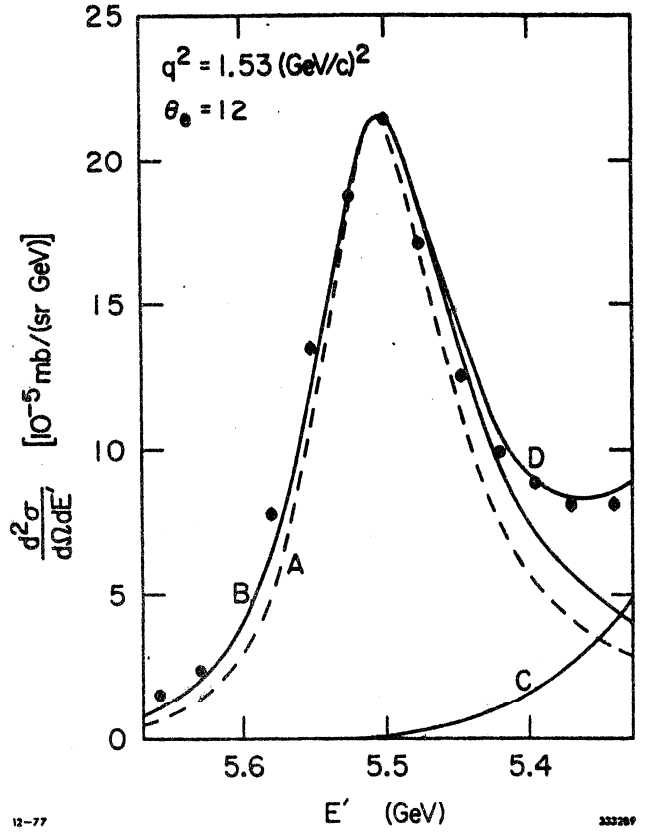

Fig. 9 Deuteron data (points) (Ref. 17) and model prediction of the quasielastic cross sections at $q^2 = 1.53\ (GeV/c)^2$. Quasielastic peak curves A and B are from Ref. 19, curve C is the inelastic processes (Ref. 18) and D is the sum. The complete figure is obtained from Ref. 17.)

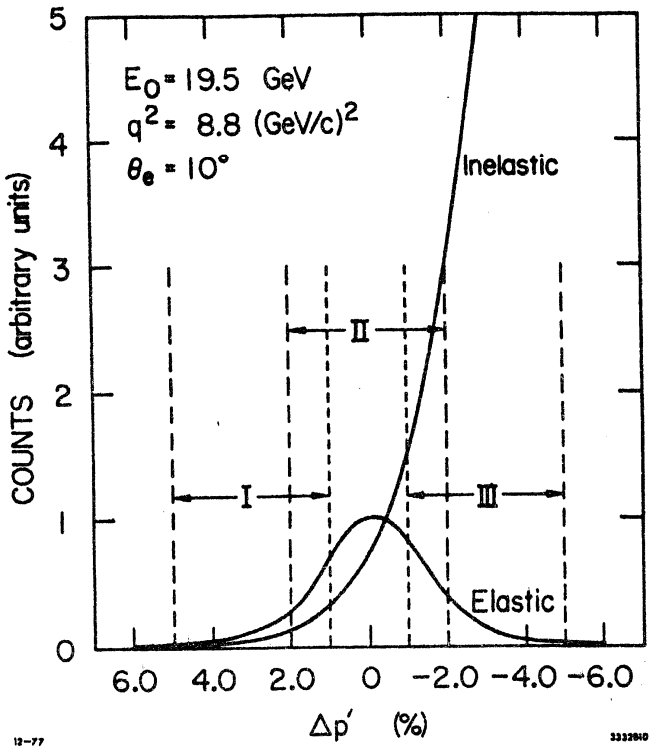

Fig. 10 The quasielastic and ineleastic scattering cross sections as a function of the scattered electron momentum at $q^2 = 8.8(\text{GeV/c})^2$. Regions I, II, and III indicate three (3) possible spectrometer field settings at fixed angle to cover the entire peak.

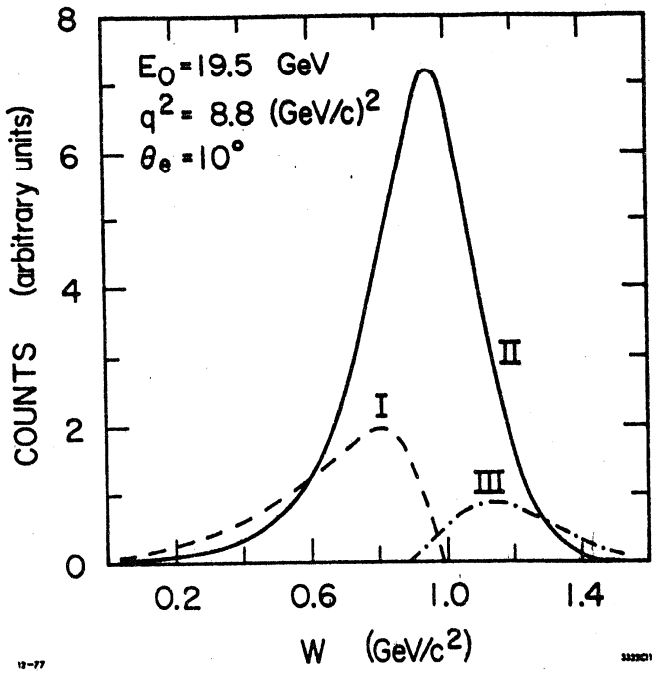

Fig. 11 Relative number of counts in the quasielastic peak regions as a function of W for three (3) settings of the spectrometer field, Regions I, II, and III of Fig. 10. Counting time in Region III is one half that of Regions I and II as explained in the text.

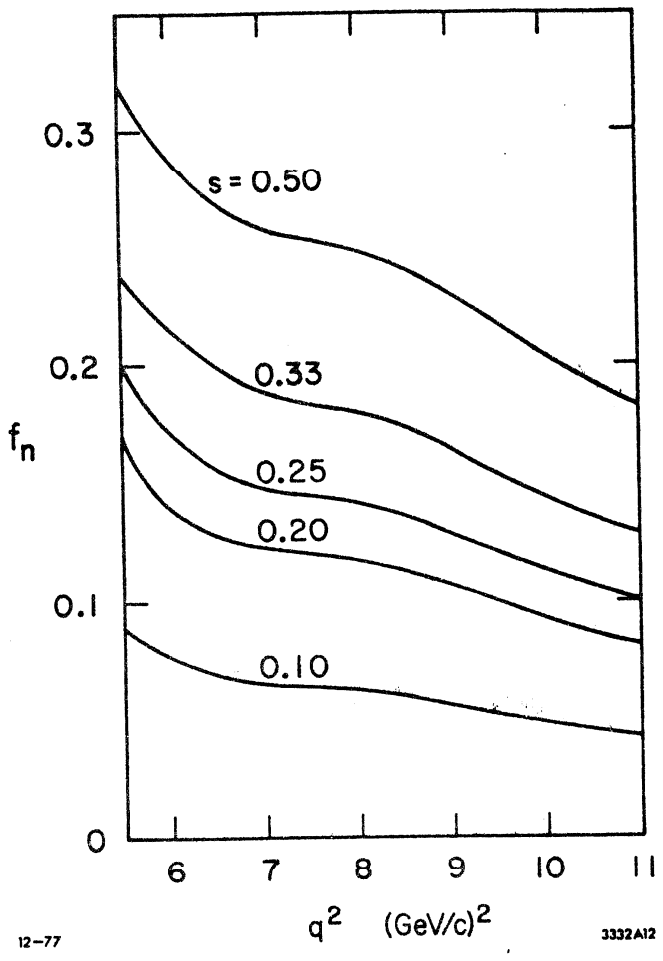

Fig. 12 Neutron fraction $f_n = \sigma_n/\sigma_{tot}$ as a function of q^2 for the Central Bin (W = .94 GeV/c^2). The different curves represent different values of $s = \sigma_n^{el}/\sigma_p^{el}$

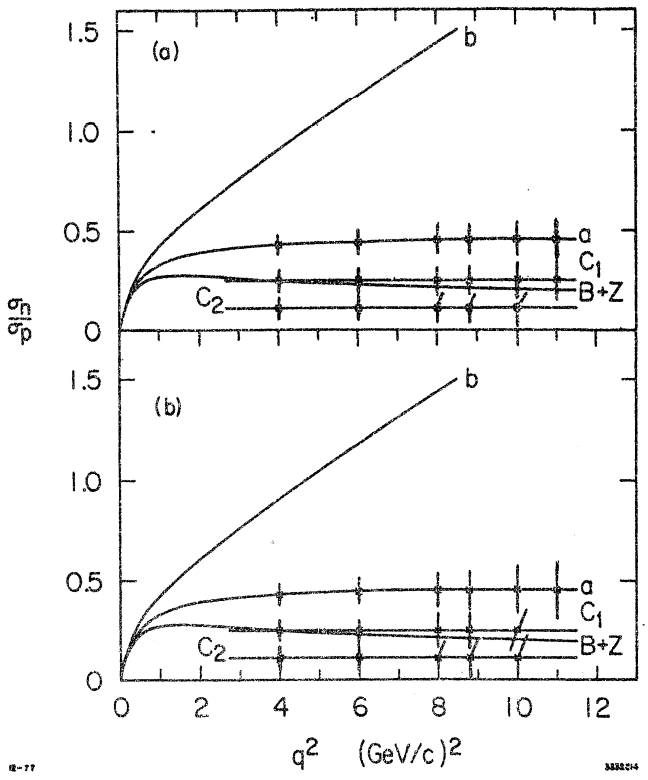

Fig. 13 Approximate errors obtainable for various values of $\sigma_n^{el}/\sigma_p^{el}$ as a function of q^2. The curves labeled a, b, c1 and c2 represent models discussed in the text. The curve B + Z is the VDM of Blatnik and Zovko (Ref. 1).

a) Background fractional error = 5%

b) Background fractional error = 10%

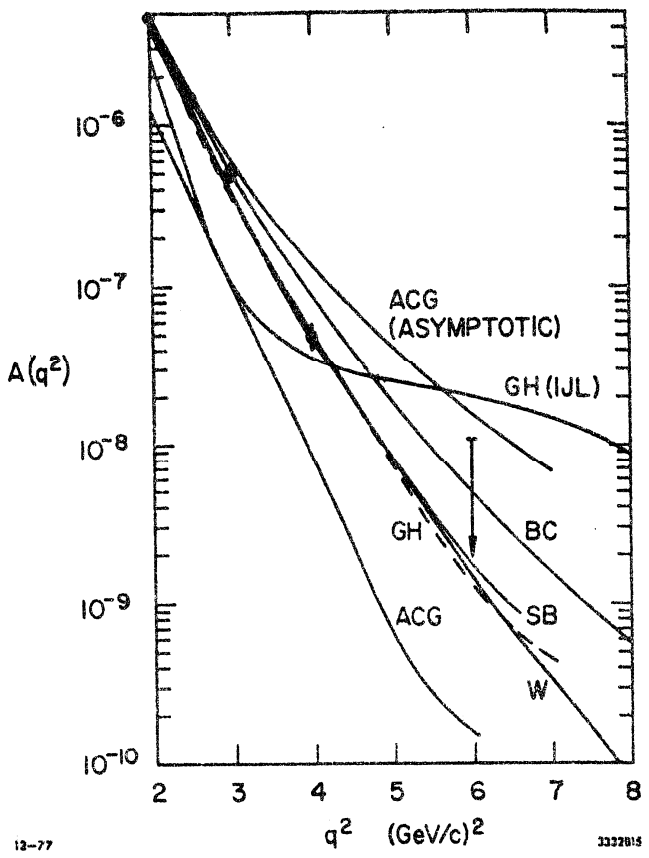

Fig. 14 Deuteron structure function $A(q^2)$ theoretical predictions and data from Ref. 20.

The curves are:

BC - Dimensional scaling Quark model of Brodsky and Chertok (Ref. 24)

GH - Nuclear physics model of Gari and Hyuga (Ref. 26) using dipole nuclear form factors

GH (IJL) - The GH model but with nuclear form factors from F. Iachello et al (Ref. 1)

ACG - Relativistic nuclear physics calculation of Arnold, Carlson and Gross (Ref. 26)

ACG (Asymptotic) = Large q^2 shape of the form factor from the ACG Calculations (Ref. 26)

SB - Relativistic nuclear physics calculation by Schmidt and Blankenbeckler (Ref. 25).

W - A prediction by West (Ref. 23)

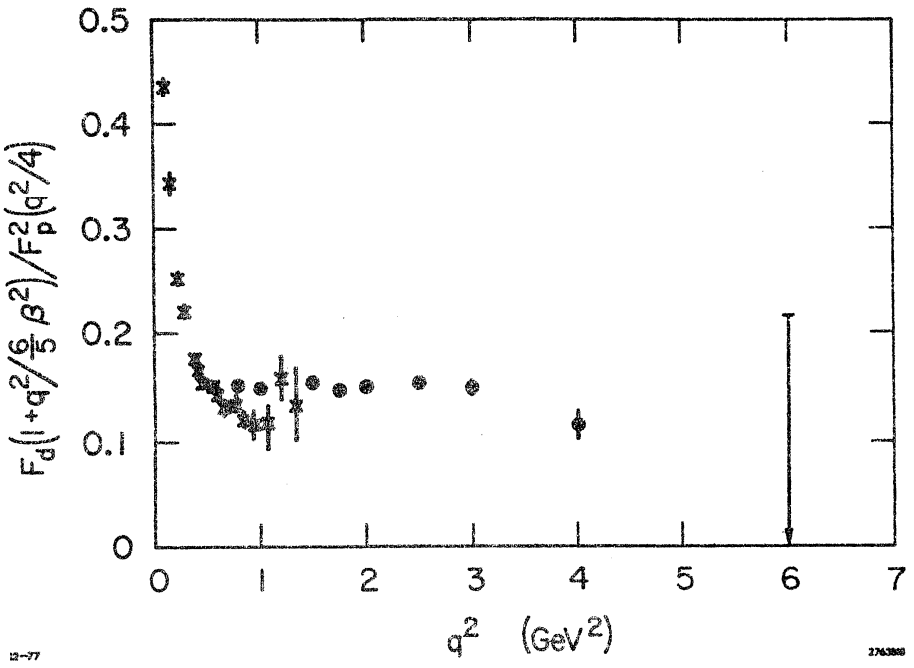

Fig. 15 Deuteron structure function A (q^2) data divided by the Dimensional Scaling Quark prediction, Eq. A1.